

This is an Open Access document downloaded from ORCA, Cardiff University's institutional repository: <https://orca.cardiff.ac.uk/id/eprint/175068/>

This is the author's version of a work that was submitted to / accepted for publication.

Citation for final published version:

Fu, Xiaopeng, Wu, Wei, Li, Peng, Mahseredjian, Jean, Wu, Jianzhong and Wang, Chengshan 2024. Splitting state-space method for converter-integrated power systems EMT simulations. IEEE Transactions on Power Delivery 40 (1) , pp. 584-595. 10.1109/tpwr.2024.3514294

Publishers page: <https://doi.org/10.1109/tpwr.2024.3514294>

Please note:

Changes made as a result of publishing processes such as copy-editing, formatting and page numbers may not be reflected in this version. For the definitive version of this publication, please refer to the published source. You are advised to consult the publisher's version if you wish to cite this paper.

This version is being made available in accordance with publisher policies. See <http://orca.cf.ac.uk/policies.html> for usage policies. Copyright and moral rights for publications made available in ORCA are retained by the copyright holders.



Splitting State-Space Method for Converter-Integrated Power Systems EMT Simulations

Xiaopeng Fu, *Member, IEEE*, Wei Wu, *Member, IEEE*, Peng Li, *Senior Member, IEEE*, Jean Mahseredjian, *Fellow, IEEE*, Jianzhong Wu, *Fellow, IEEE*, and Chengshan Wang, *Senior Member, IEEE*

Abstract—As the utilization of power electronic-based components in power systems continues to grow, a comprehensive understanding of their dynamics becomes increasingly important for system design, control and protection analysis. To meet practical needs, the high-fidelity but time-consuming electromagnetic transient (EMT) simulations are often required. To improve the performance of these simulations, a highly efficient splitting state-space method with numerical error control is proposed that reduces the computation workload. The method employs a generic decoupling principle to split the state-space equations of the converter-integrated power system and introduces the exponential splitting formulas of multiple orders accuracy to solve and then compose the splitting state-space equations. The decoupling principle is designed based on separation of time-varying portions of the state matrix, which is realized by locating the smallest subcircuit topology that is switch state-dependent, through automatic switch grouping and switch adjacent state variables (SASV) identification. A family of exponential splitting schemes is employed to accelerate the demanding matrix exponential calculation. The splitting state-space method undergoes comprehensive testing across various cases, including a distribution network with DC load, an LLC resonant converter, a large-scale wind farm, and an MMC circuit. The accuracy of the proposed method is thoroughly evaluated, and its efficiency is validated.

Index Terms—Electromagnetic transient, exponential integrator, power converter, splitting method.

I. INTRODUCTION

THE power systems are becoming increasingly complex due to renewable generation penetration and hybrid ac/dc network interconnections, which lead to widespread utilization of power electronic-based converters [1]. This complexity has a profound impact on the system dynamic performance, and raises the need for accurate time-domain simulation of power system transients [2]. Electromagnetic transient (EMT) simu-

lation programs, which adopt the detailed modeling approach, can provide high-fidelity simulation results at the circuit level. Previously, these programs were mainly used to track the fast EMT phenomenon that is naturally confined to local area, but growing demands from practical studies in longer timespan and larger scale were seen more recently. For example, diverse coupling forms among power electronic converters and traditional electrical equipment are observed to trigger wide-band oscillations [3]. Cross-region interactions are formed between energy plants and load center networks through long distance DC transmission systems [4]. These demands pose new challenges to EMT simulation programs. The ever-increasing advancement of high-switching-frequency (HSF) converters has notably resulted in semiconductor valve switching frequencies reaching hundreds of kilohertz [5], requiring small enough time-steps to capture the switching dynamics. This requirement also arises from the small-time constants associated with the component dynamics and device transients with nonlinear characteristics. The increasing number of converters in the power system and the stringent simulation requirements impose higher demands on the execution time and computing resources required for these simulations.

Various techniques aimed at improving the efficiency of detail-modeled power converter simulations have been developed in earlier studies. Circuit-based decoupling, as one common idea, has been adopted by methods like multirate analysis and parallel computations to accelerate the simulations [6], [7]. Circuit decoupling is conventionally achieved by transmission line propagation delay, while the compensation method can be used to decouple at arbitrary locations where line delays are not available [8]. The state-space nodal method (SSN) is also able to avoid line delay usage by interfacing nodal analysis equations with grouped state-space equations, where the grouping splits switching events and reduces the computation burden related to varying topology matrix calculations [9]. A circuit partitioning method was presented in [10] that applied an explicit formula to selected energy storage elements for power electronic circuit division and used multirate methods to improve efficiency. In [11], a region folding method decoupled the identical structural power electronic blocks to precalculate their inverse matrices. Further investigations are needed for efficient decoupling methods that can be applied to generic power converter topologies.

One merit of the decoupling methods is that they alleviate the explosion of the involved switch on/off state combination

This work was supported by National Key R&D Program of China under Grant 2023YFC3807000, and National Natural Science Foundation of China under Grant 52377118. (*Corresponding Author: Wei Wu*).

Xiaopeng Fu, Peng Li, and Chengshan Wang are with the Key Laboratory of Smart Grid of Ministry of Education, Tianjin University, Tianjin 300072, China (e-mail: fuxiaopeng@tju.edu.cn, lip@tju.edu.cn, cswang@tju.edu.cn).

Wei Wu is with Beijing Huairou Laboratory, Beijing 102206, China (e-mail: wuweil@neps.hrl.ac.cn).

Jean Mahseredjian is with the Department of Electrical Engineering, Polytechnique Montréal, Montréal, Québec H3T 1J4, Canada. (e-mail: jeanm@polymtl.ca).

Jianzhong Wu is with the Institute of Energy, School of Engineering, Cardiff University, Cardiff CF24 3AA, U.K. (e-mail: wuj5@cardiff.ac.uk).

numbers by appropriate switch separation into subsystems. Apart from this, constant admittance matrix or state matrix methods to approximate the switching state/model have also drawn attention. A buck converter was modeled using a piecewise-linear approximation in [12], which separated the nonlinear switch property into several subsections and obtained a constant admittance matrix. The associated discrete circuit models were developed to maintain constant admittance with different passive element representations during on/off states [13], and have been used for boost/buck inverters, three-level voltage source converter (VSC), etc., especially in real-time applications [14], [15]. The insulated gate bipolar transistor (IGBT) and its parallel diode were modeled as a voltage-current source pair in [16], and one time-step latency was introduced to achieve an invariant coefficient matrix. Various modeling techniques for modular multilevel converters (MMCs) are presented in [17].

In contrast to the circuit-based decoupling and constant matrix approaches, this paper proposes a splitting state-space method with numerical error control scheme. The foundation of the method is a decoupling principle applicable for general converter topology, which extracts the time-varying part of the state-space equations of the converter-integrated power systems and generalizes the matrix structure of this part, hence splitting the state-space equations. Consequently, the method mitigates the computational burden associated with switch operations. On this basis, the method employs the exponential splitting formulas to adaptively execute the numerical integration of time-varying and constant parts separately. Last but not least, the method provides flexible options for solutions of each accuracy order, and uses a numerical error control scheme to guide this setting, which helps in balancing the trade-off between simulation accuracy and efficiency, enhancing the overall performance.

The remainder of the paper is organized as follows. Section II introduces the splitting state-space method and its numerical error control scheme. Section III demonstrates the decoupling principle with typical converter topologies. Section IV presents several case studies to examine the performance of the proposed method. Conclusions are drawn in Section V.

II. SPLITTING STATE-SPACE METHOD

The ordinary differential equations (ODEs) describing converter-integrated power systems are time-varying due to the switch operations, and the numerical integration of the ODEs can be computationally intensive. The splitting state-space method proposed in this section is aimed to address this challenge. For the post-switching update of the state-space equations, this method first identifies the pattern of elements in the state matrix and splits the equations into time-varying and constant parts. Then, by incorporating the exponential splitting formulas of multiple orders accuracy, the solutions to the splitting state-space equations and their composition are derived to approximate the solution of the full state-space equations. The integration in each time-step is accordingly divided into several stages, and the computation of the exponential of the entire time-varying state matrix is avoided. The method also consid-

ers the accuracy loss induced by the splitting state-space method and provides error control scheme.

A. Exponential Splitting Formulas

An N -dimensional linear system has the state-space form

$$\dot{\mathbf{x}} = \mathbf{A}\mathbf{x} + \mathbf{B}\mathbf{u}, \quad \mathbf{x}(0) = \mathbf{x}_0, \quad (1)$$

where \mathbf{x} and \mathbf{u} denote the vector of state variables and input variables, \mathbf{A} and \mathbf{B} are the state and input matrices that represent the coefficients of the system, and \mathbf{x}_0 is the initial value of \mathbf{x} . For easier presentation, a convenient technique from [18] is used to transform this non-autonomous system form into an augmented and autonomous form

$$\dot{\tilde{\mathbf{x}}} = \tilde{\mathbf{A}}\tilde{\mathbf{x}}, \quad (2)$$

where the effect of the forcing term \mathbf{u} is wrapped into the augmented state vector $\tilde{\mathbf{x}}$, which contains the original \mathbf{x} and auxiliary state variables \mathbf{x}_u . This technique can be exemplified by transforming a simple system with constant input c , $\dot{\mathbf{x}} = \mathbf{A}\mathbf{x} + \mathbf{b}c$, by defining $\tilde{\mathbf{A}} = \begin{bmatrix} \mathbf{A} & \mathbf{b} \\ \mathbf{0} & 0 \end{bmatrix}$, $\tilde{\mathbf{x}} = \begin{bmatrix} \mathbf{x} \\ \mathbf{x}_u \end{bmatrix}$, and $\tilde{\mathbf{x}}(0) = \begin{bmatrix} \mathbf{x}_0 \\ c \end{bmatrix}$. The equivalence of (1) and (2) can be easily demonstrated and such a transformation is available for different input signal forms. The state transition rule for system (2) is explicitly expressed with the matrix $\tilde{\mathbf{A}}$ exponential function as

$$\tilde{\mathbf{x}}(t) = \mathbf{e}^{\tilde{\mathbf{A}}t}\tilde{\mathbf{x}}(0). \quad (3)$$

In the following presentation, we use (3) as the fundamental equation describing the system dynamics, and the tilde superscript is dropped for concise notation. This formulation is general, as the forcing term is included in the auxiliary state variables.

Numerical integration with the exponential integrators [19] involves the computationally intensive matrix exponential function with a time complexity of $O(N^3)$, which becomes the efficiency bottleneck in the converter-integrated power systems EMT simulations. The exponential splitting formulas can treat these matrix operations more easily [20]. The method consists of three steps, which are decoupling, integration and combination. In the first step, the system is decoupled and the state matrix \mathbf{A} is split into two matrices $\mathbf{A} = \mathbf{A}_1 + \mathbf{A}_2$. It is noted that this paper uses *italic symbol* to denote time-varying vectors and matrices, to better distinguish those data structs that vary with switch states from those that do not. Then, the exponential of \mathbf{A} is approximated with splitting formulas as product of matrix exponentials formed by \mathbf{A}_1 and \mathbf{A}_2 . Among them, the first-order accurate Trotter formula is [21]

$$\mathbf{e}^{h(\mathbf{A}_1+\mathbf{A}_2)} = \mathbf{e}^{h\mathbf{A}_1}\mathbf{e}^{h\mathbf{A}_2} + O(h^2), \quad (4)$$

where h is integration time-step. The approximation error of (4) is second-order of h by comparing their Taylor expansions $\mathbf{e}^{h(\mathbf{A}_1+\mathbf{A}_2)} - \mathbf{e}^{h\mathbf{A}_1}\mathbf{e}^{h\mathbf{A}_2}$

$$= (\mathbf{I} + h(\mathbf{A}_1 + \mathbf{A}_2) + h^2(\mathbf{A}_1 + \mathbf{A}_2)^2/2 + O(h^3)) - (\mathbf{I} + h\mathbf{A}_1 + h^2\mathbf{A}_1^2/2 + O(h^3))(\mathbf{I} + h\mathbf{A}_2 + h^2\mathbf{A}_2^2/2 + O(h^3)) - h^2(\mathbf{A}_2\mathbf{A}_1 - \mathbf{A}_1\mathbf{A}_2)/2 + O(h^3). \quad (5)$$

For higher-order approximations, a recursive way to construct exponential product formula is given in [22]. By symmetrizing (4) and eliminating even-order correction terms, the approximation is promoted to second-order accurate [23]

$$\mathbf{e}^{h(\mathbf{A}_1+\mathbf{A}_2)} = \mathbf{e}^{\frac{h}{2}\mathbf{A}_2}\mathbf{e}^{h\mathbf{A}_1}\mathbf{e}^{\frac{h}{2}\mathbf{A}_2} + O(h^3). \quad (6)$$

The splitting exponentials product is of a simpler type than its original counterpart, as the exponential of the constant part \mathbf{A}_1 is calculated only once, while the time-variant part \mathbf{A}_2 is sparser than the original state matrix, and its exponential can be calculated efficiently with sparse methods.

The state-space equation of a converter-integrated power system can be rewritten in the block matrix form

$$\begin{bmatrix} \dot{\mathbf{x}}_1 \\ \dot{\mathbf{x}}_2 \end{bmatrix} = \begin{bmatrix} \mathbf{A}_{11} & \mathbf{A}_{12} \\ \mathbf{A}_{21} & \mathbf{A}_{22} \end{bmatrix} \begin{bmatrix} \mathbf{x}_1 \\ \mathbf{x}_2 \end{bmatrix}, \quad (7)$$

where \mathbf{x}_2 denotes the state variables of converter switch adjacent components, therefore, the state equations of \mathbf{x}_2 contain switch state-dependent terms, and \mathbf{x}_1 represents the other state variables. Since the topology of the switch-independent subcircuit remains constant, the submatrices \mathbf{A}_{12} , \mathbf{A}_{21} and \mathbf{A}_{11} are constant. The submatrix \mathbf{A}_{22} is time-variant and made up of N_C subdivisions corresponding to N_C converters, as shown in Fig. 1, the time-varying elements in \mathbf{A}_{22} are located in the diagonal blocks \mathbf{g}_i associated with the i^{th} converters. This is due to converters are separated by components such as filters and lines, and there is no direct connection in between. Therefore, the time-varying elements can be managed for each individual converter. In addition, the structure helps to streamline the decoupling procedure.

The state matrix splitting of such system is detailed in Fig. 1. The state matrix \mathbf{A} can be split into a constant splitting matrix \mathbf{A}_1 , and a block-wise variant splitting matrix \mathbf{A}_2 that depends on the switch states \mathbf{s} at time t , it is noted as $\mathbf{A}_2(\mathbf{s}(t))$ in this subsection. Mapping the splitting of the state matrix to real circuits, integrations of subcircuits represented by \mathbf{A}_1 obtain the system transients without power conversion through converters, on the other hand, integrations of subcircuits represented by $\mathbf{A}_2(\mathbf{s}(t))$ complement this part of power conversion. Using the exponential splitting formulas, the exponential of \mathbf{A}_1 is determined in the beginning of the simulation and remains constant, while the exponential of the counterpart $\mathbf{A}_2(\mathbf{s}(t))$ is approximated in practical calculations once the switch states change, where the approximation is designed match the accuracy order of the exponential splitting formula. Given that the aim of the splitting state-space method is to reduce the computation effort, the Taylor series expansion is adopted in this paper to approximate the exponential of $\mathbf{A}_2(\mathbf{s}(t))$ because it is efficient to implement.

With the approximation of the exponential product of splitting matrices, the proposed method splits the integration procedure into several sub-steps. Trotter formula (4) splits each integration step into two sub-steps.

$$\begin{cases} \mathbf{x}'_n = \mathbf{f}_1(\mathbf{h}\mathbf{A}_2(\mathbf{s}(t_n)))\mathbf{x}_n, \\ \mathbf{x}_{n+1} = \mathbf{e}^{\mathbf{h}\mathbf{A}_1}\mathbf{x}'_n \end{cases}, \quad (8)$$

where \mathbf{x}'_n is the vector of intermediate state variables in $[t_n, t_{n+1}]$, and $\mathbf{f}_k(\mathbf{h}\mathbf{A}_2(\mathbf{s}(t_n)))$ denotes the summation of the first $k + 1$ terms of a Taylor series of exponential function.

$$\mathbf{f}_k(\mathbf{h}\mathbf{A}_2(\mathbf{s}(t_n))) = \sum_{i=0}^k \frac{1}{i!} (\mathbf{h}\mathbf{A}_2(\mathbf{s}(t_n)))^i. \quad (9)$$

Other schemes for splitting integration exist, e.g., with the Trotter formula and the constant subsystem integrated first rather than its counterpart in (8). These two schemes have

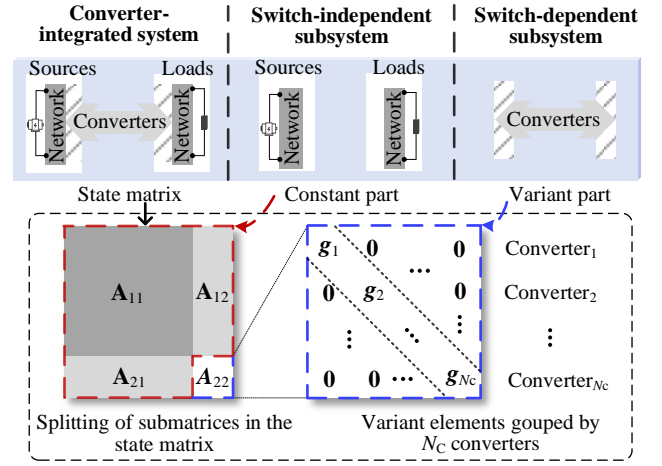


Fig. 1 Splitting state matrix for the converter-integrated power systems.

opposite second-order correction terms. Furthermore, using the higher-order accurate exponential splitting formula (6), the integration is split into three sub-steps shown in (10), in which the switch-dependent subsystem is integrated in the first and third sub-steps for a halved time-step size, and the constant subsystem is integrated for a full time-step in between

$$\begin{cases} \mathbf{x}'_n = \mathbf{f}_2\left(\frac{\mathbf{h}}{2}\mathbf{A}_2(\mathbf{s}(t_n))\right)\mathbf{x}_n \\ \mathbf{x}''_n = \mathbf{e}^{\mathbf{h}\mathbf{A}_1}\mathbf{x}'_n \\ \mathbf{x}_{n+1} = \mathbf{f}_2\left(\frac{\mathbf{h}}{2}\mathbf{A}_2(\mathbf{s}(t_n))\right)\mathbf{x}''_n \end{cases} \quad (10)$$

where \mathbf{x}''_n is also a vector of intermediate state variables.

The implementation of the formula (10) is drawn in detail, as shown in Fig. 2, the matrix \mathbf{A} is presented in the blocked form as in (7), so that the constructure of the matrix \mathbf{A}_1 and $\mathbf{A}_2(\mathbf{s}(t))$ is convenient given. In the sub-steps ① and ③, the switch-dependent subsystem is integrated, updating only the subset of state variables \mathbf{x}_2 , and the exponentials of the submatrix \mathbf{A}_{22} . Therefore, the method reduces the computational workload, and has potential for simulating massive switch operations.

B. Accuracy Control of Splitting State-Space Method

To determine the applicability of the splitting state-space method for EMT simulations, it is necessary to evaluate its induced error analytically. By deriving and analyzing the matrix of local error of the presented exponential splitting scheme, some key information can be obtained before running EMT simulations. Feasible simulation time-step size and the exponential splitting formulas can be assessed. For this reason, a criterion for the evaluation is proposed in this subsection. The global error can be approximately controlled by the local error,

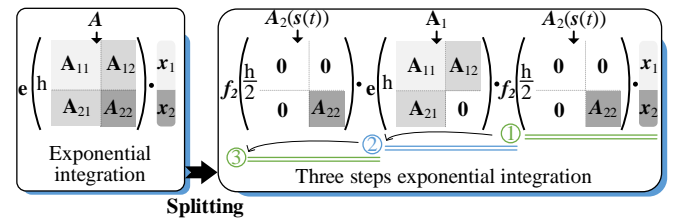


Fig. 2 Splitting exponential integration procedure

and the reliability of error approximations can be augmented through the step-size adjustment based on local error control [24]. To estimate the local error, it is reminded that the dominant error term \mathbf{E}_2 of the first-order exponential splitting formula (4) has been established in (5) as

$$\mathbf{E}_2 = h^2(\mathbf{A}_2\mathbf{A}_1 - \mathbf{A}_1\mathbf{A}_2)/2. \quad (11)$$

Similarly, the dominant error matrix of second-order exponential splitting is denoted as \mathbf{E}_3 , and the m -order error matrix as \mathbf{E}_m . Then, the local error introduced by the exponential splitting formula is represented with \mathbf{E}_m . In addition, the local error introduced by the approximate of the time-varying matrix exponential $\mathbf{f}_k(h\mathbf{A}_2(\mathbf{s}(t_n)))$ is represented with \mathbf{E}_t . Taking the Trotter formula and the first two terms of a Taylor series of exponential function as an example, \mathbf{E}_t is

$$\mathbf{E}_t = \mathbf{e}^{h\mathbf{A}_1}\mathbf{f}_1(\mathbf{e}^{h\mathbf{A}_2}) - \mathbf{e}^{h\mathbf{A}_1}\mathbf{e}^{h\mathbf{A}_2} = h^2\mathbf{A}_2^2/2 + 0(h^3). \quad (12)$$

The splitting error matrix \mathbf{E}_s is defined as

$$\mathbf{E}_s = \mathbf{E}_m + \mathbf{E}_t. \quad (13)$$

Since the matrix norm is guaranteed to be compatible with the vector norm, the error estimation can be regarded as the measure of the matrices in (13). The logarithmic norm is introduced as the tool for matrix measure [25]

$$\mu(\mathbf{A}) = \lim_{h \rightarrow 0^+} \frac{\|\mathbf{I} + h\mathbf{A}\| - 1}{h}, \quad (14)$$

where $\|\cdot\|$ denotes the vector norm in \mathbb{R}^n and the corresponding induced matrix norm in $\mathbb{R}^{n \times n}$, and \mathbf{I} is the identity matrix.

Within the time-step $[t_n, t_{n+1}]$, the m -order splitting error S_m is denoted as $\mu(\mathbf{E}_s\mathbf{x}_n)$.

$$\mu(\mathbf{E}_s\mathbf{x}_n) \leq \mu(\mathbf{E}_m\mathbf{x}_n) + \mu(\mathbf{E}_t\mathbf{x}_n) \quad (15)$$

It can be assumed that $\mu(\mathbf{A}) \approx \mu(\mathbf{A}_1) = a$ and $\mu(\mathbf{A}_2) = b(s(t))$, where a is a constant parameter and $b(s(t))$ is varying with the switch state [26].

Since $b(s(t))$ is time-variant as the matrices in (15) change with the switch states, an exhaustive set of switch states seems necessary for the computation. Fortunately, the identification of the upper bound of S_m could simplify the analytical process. The upper bound of S_m is analyzed based on the binary resistances switch model, where the associated switch elements exhibit considerable magnitude due to the resistance in the off-state when all converter switches are turned off, and the estimated splitting error with the off-state switches has the maximum value S_m among all switch states. Since the upper bound of the splitting error is analyzed based on the binary resistances switch model, where the associated switch elements exhibit considerable magnitude due to the resistance in the off-state when all converter switches are turned off, and the estimated splitting error with the off-state switches has the maximum value S_E among all switch states. The logarithmic norm of \mathbf{A}_2 with the off-state switches is defined as b_0 , and given that the components corresponding to the SASVs typically possess relatively large inertia, it can be assumed that $b_0/a \ll 1$.

Substituting (11) and (12) into equation (15), the first-order splitting error S_1 is

$$S_1 \approx h^2ab_0. \quad (16)$$

The second-order splitting error can be derived from (10) and (15). Then, a threshold t_E is introduced to make sure the m -order splitting error S_m is small. to estimate the local error,

and is bounded by the threshold t_E .

$$S_m < t_E. \quad (17)$$

The calculation of S_m can be efficiently performed on a range of simulation time-step h and the order of exponential splitting formulas. Following the ascertainment of S_m , the optimization of simulation settings, based on the local error control of (17), can be executed before the simulation starts. Once the exponential splitting formula is selected, a range of simulation time-step can be estimated. Alternatively, when a specific size of the time-step is required, the error control tells the applicability of the splitting state-space method for specific cases.

III. DECOUPLING PRINCIPLE FOR POWER CONVERTERS

For converter-integrated power systems, the dimension of state matrix and the number of its possible variants due to the switch state-dependent nature are seeing an increase, and it is resource-expensive to always reformulate the whole matrix. One of the advantages of the state-space method is that all the time-varying state matrix elements lie in the corresponding rows and column vectors of certain switch-adjacent components. This recognition of the time-varying elements is the primary motivation for applying the splitting state-space method. To this end, a decoupling principle that automatically extract these time-varying matrix portions from the power converter circuits is set forth in this section. This principle serves as the guide for the first step of the splitting state-space method. Furthermore, the decoupling principle is applicable to general converter topologies.

A. Automated State Matrix Decoupling Procedures

Firstly, the decoupling principle is elaborated using a half-bridge converter circuit as an example, as shown in Fig. 3. Source side DC circuit is connected to the converter through the nodes n_1 and n_2 , source side AC circuit is connected to the converter through the nodes n_3 and n_0 . The IGBTs g_1, g_2 and their anti-parallel diodes d_1, d_2 share nodes from switch nodes set $\mathbf{N}_s = \{n_1, n_2, n_3\}$. The state variables are the inductor current I_L and the capacitor voltages U_{C1} and U_{C2} .

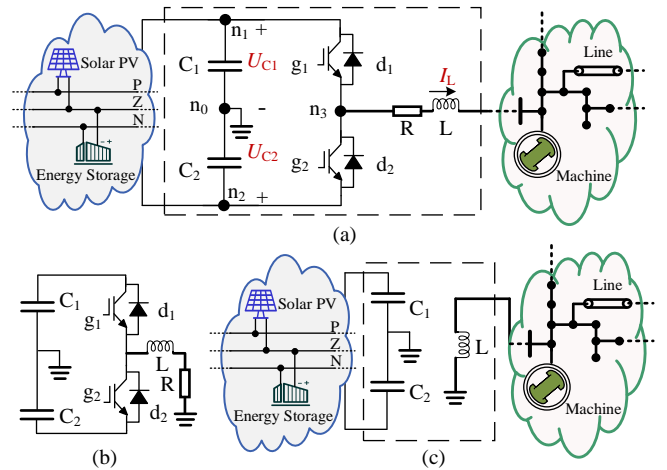


Fig. 3 Half-bridge converter circuit for demonstrating the decoupling principle: (a) half-bridge circuit, (b) subcircuit of the time-varying splitting matrix, (c) subcircuit of the constant splitting matrix.

To realize the decoupling, power electronic switches are first grouped based on their corresponding converters. Switches that share nodes from the same \mathbf{N}_s are designated into one group. Since different converters are inherently decoupled from each other, this facilitates the dependent procedures across groups and possesses potential parallelism. The state variables of capacitors and inductors that are connected to all \mathbf{N}_s sets, referred to as switch adjacent state variables (SASV) in this paper, are then readily determined. In the case of Fig. 3, the state equations of the SASV are dependent on the turn on/off state functions S_1 and S_2 of the switch pairs g_1/d_1 and g_2/d_2 , where S_1 and S_2 have values 1/0 for the turn on/off states. In this circuit, I_L and U_{C1} , U_{C2} are identified as SASV.

In essence, only the coefficients of SASV in the state equations change along with the switch operations inside the converters. The half-bridge converter circuit can be decoupled into two subcircuits, which describe the switch-dependent and constant equations respectively. The corresponding state equations of the switch-dependent and independent subcircuits are given in (18) and (19), where \mathbf{A}_{C1} , \mathbf{A}_{C2} , \mathbf{A}_L and \mathbf{A}_n are coefficient matrices, \mathbf{a}_{C1} , \mathbf{a}_{C2} and \mathbf{a}_L are coefficient vectors, \mathbf{x}_1 is the vector of state variables represent the circuits outside the converter. The inductor L has the series resistor R, and the pivot element $-R/L$ corresponding to I_L in (18) is constant, because when the inductors corresponding to the SASVs have series resistors or when the capacitors have parallel resistors, the diagonal elements corresponding to the SASVs are constants, correlating with the respective resistance values. It is still maintained in (18) to ensure consistency of the method. Since the circuit is not included in the switch-dependent subcircuit, the derivative of \mathbf{x}_1 in (18) is zero.

$$\begin{bmatrix} \dot{\mathbf{x}}_1 \\ \dot{U}_{C1} \\ \dot{U}_{C2} \\ \dot{I}_L \end{bmatrix} = \begin{bmatrix} \mathbf{0} & \mathbf{0} & \mathbf{0} & \mathbf{0} \\ \mathbf{0} & 0 & 0 & -S_1/C_1 \\ \mathbf{0} & 0 & 0 & -S_2/C_2 \\ \mathbf{0} & S_1/L & S_2/L & -R/L \end{bmatrix} \begin{bmatrix} \mathbf{x}_1 \\ U_{C1} \\ U_{C2} \\ I_L \end{bmatrix}, \quad (18)$$

$$\begin{bmatrix} \dot{\mathbf{x}}_1 \\ \dot{U}_{C1} \\ \dot{U}_{C2} \\ \dot{I}_L \end{bmatrix} = \begin{bmatrix} \mathbf{A}_n & \mathbf{a}_{C1} & \mathbf{a}_{C2} & \mathbf{a}_L \\ \mathbf{A}_{C1} & 0 & 0 & 0 \\ \mathbf{A}_{C2} & 0 & 0 & 0 \\ \mathbf{A}_L & 0 & 0 & 0 \end{bmatrix} \begin{bmatrix} \mathbf{x}_1 \\ U_{C1} \\ U_{C2} \\ I_L \end{bmatrix}. \quad (19)$$

To explain this method from the perspective of physical circuits, the subcircuits described by the splitting state equations are presented in Fig. 3(b) and (c). To form the constant part subcircuit, the current injections into SASV capacitors from the converter switch branches are set to zero, thus these branches are replaced by open circuits, while other branches remain unchanged. The voltages of switch-adjacent terminal of SASV inductors are set to zero, therefore the shared nodes of the converter switches and SASV inductors are grounded, while other nodes remain unchanged. The formulation of time-varying part subcircuits is complementary to the constant part subcircuits. Comparing the circuits in Fig. 3, the capacitors C_1 and C_2 are charged and the inductor L is discharged in the constant part subcircuit. The power conversions among those energy storage elements represented by SASV are carried out in the switch-dependent subcircuit, where C_1 and/or C_2 charges L through the switch pairs.

Based on the above analysis, the procedure of the decoupling principle for the splitting state-space method is summarized in Fig. 4. First the system dimension and power electronic switch number are estimated to evaluate the necessity of splitting the state-space matrix. For systems containing multiple power electronic switches, all switches are then classified into N_C switch groups in a topology scan, and the switch group node sets \mathbf{N}_s are formed. For each switch group, the SASV are identified which are capacitor voltages and inductor currents connected to \mathbf{N}_s nodes. The branches and nodes can be replaced with open and short circuits, respectively, to obtain the decoupled subcircuits. Notably, when the inductors corresponding to the SASVs have series resistors or when the capacitors have parallel resistors, the corresponding resistors are included within the subcircuit of the time-varying splitting matrix. Last but not least, the splitting state matrices corresponding to the switch-dependent subcircuits are formulated. These decoupled subcircuits are much smaller than the original circuits, enabling computationally efficient state-space matrix derivation and easy integration into the numerical procedure of the splitting state-space method.

B. Demonstration on Typical Converter Topologies

The presented decoupling principle is general and not limited to any particular convert topology. This section will supplement two examples of decoupling typical converter topologies, including a Cuk converter and an MMC circuit, but not with very detailed explanation.

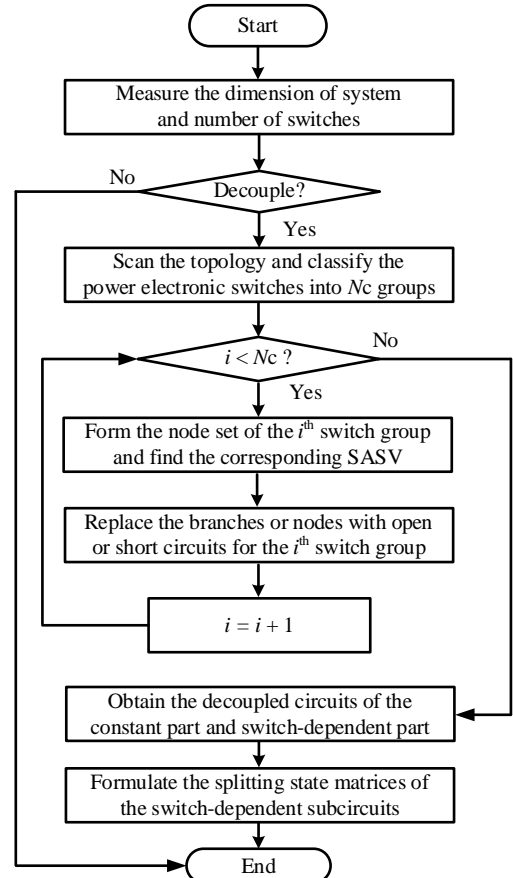


Fig. 4 Flowchart of the decoupling procedure.

A Cuk converter case is shown in Fig. 5. The IGBT g and the diode d share the common nodes from the switch nodes set $\mathbf{N}_s = \{n_0, n_1, n_2\}$. SASV of this switch group are the capacitor C_1 voltage and inductor L_1 and L_2 currents. Following the presented procedure, decoupled subcircuits are derived as in Fig. 5(b) and (c).

For the MMC converter as depicted in Fig. 6 (a), the power electronic switches including the IGBTs g_1 and g_2 and anti-parallel diodes d_1 and d_2 inside the Sub-Modules (SMs) from the upper arm are categorized as one group, and those from the lower arm are categorized as another group. For symmetry of the two arms, only the decoupling of the upper arm is presented here. Firstly, the SASVs are SM capacitor voltages and the upper arm inductor L_1 current. The capacitor current in

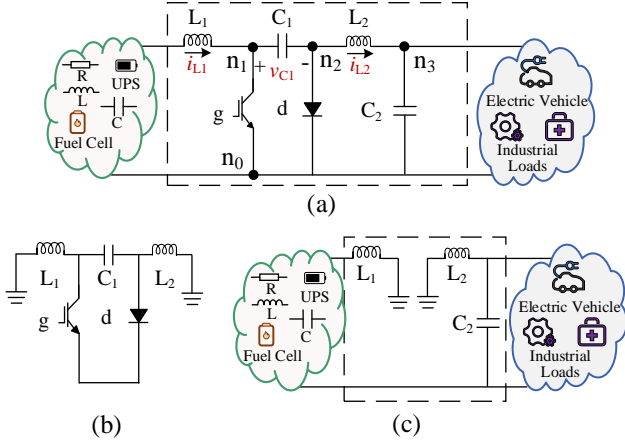


Fig. 5 Cuk converter: (a) circuit diagram, (b) subcircuit of the time-varying splitting matrix, (c) subcircuit of the constant splitting matrix.

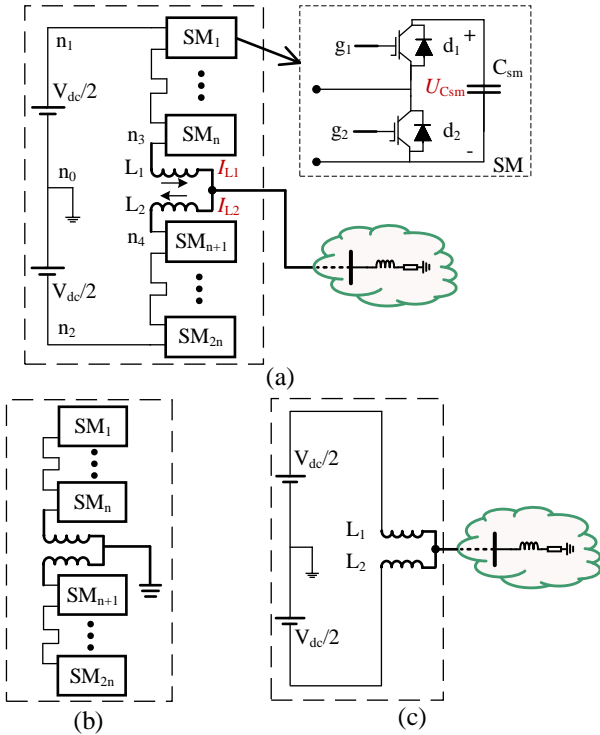


Fig. 6 MMC converter with half-bridge submodules: (a) circuit diagram, (b) subcircuit of the time-varying splitting matrix, (c) subcircuit of the constant splitting matrix.

each SM is zero or equals to the L_1 current depending on if the SM capacitor is bypassed. The L_1 voltage totally depends on the number of inserted SMs. The decoupled subcircuits are drawn in Fig. 6(b) and (c).

It is noted that for MMC there exists more specialized reduced-order equivalent model in the nodal analysis-based programs [27]. It is rooted in static circuit principle and derived by analysis of specific topology, not applicable to state-space models. The presentation here does not intend to compete with these specialized models, but to show the action of the decoupling principle on high-power converter systems containing series/parallel modules, with MMC as an example. Quantitative tests on MMC are included in section IV.D. The proposed method is developed with dynamic system theory and differential equation model, and is general-purpose for convert topologies. The readers are invited to test on other converters of interest.

The merit of the presented decoupling procedure is three-fold. First, it is differential equation theory-based with rigorous error quantification, in contrast to circuit-based approaches that are empirical. Secondly, the decoupling principle has clear physical interpretation from the viewpoint of decoupled subsystem equivalent circuits, which match different power conversion stages. It is a more sophisticated dynamical representation of the physical process than previous approaches that commonly assumes some interface variables of inertia components remaining constant during fixed periods. Last but not least, an algorithmic procedure is available and programmed for automatic decoupling without user effort and intervention.

IV. CASE STUDY

In this section, the splitting state-space method and the decoupling principle are applied to a distribution network with DC load, a 500 kHz LLC resonant converter circuit, a type-4 wind turbine generator-based wind farm, and an MMC circuit to verify the accuracy and efficiency by comparing simulation waveforms with EMTP® [28].

A. IEEE-13 Node System with DC Load

The IEEE-13 node system with DC load in Fig. 7 is first tested with the splitting state-space method. The diode bridge is modeled with ideal diode model with 0.7 V ignition voltage. The number of state variables of the system is 74. The simulation lasts for 5 s with a time-step of 10 μ s. EMTP results with a smaller 5 μ s time-step is taken as the benchmark. The state matrix is split between the phase-A inductor L_1 and DC load capacitor C_1 . Fig. 8 presents the inductor L_1 current waveforms, which are obtained by the accurate matrix exponential integrator (Exp) scheme, the splitting matrix exponential integrator (sExp) scheme, and EMTP, respectively.

Three splitting schemes are tested:

1. the first-order Trotter formula that integrates the constant part first (sExp-1st-12);
2. the first-order Trotter formula that integrates the switch-dependent variant part first (sExp-1st-21);
3. the second-order Strang formula (sExp-2nd).

The sExp-2nd scheme gives the best accuracy, followed by

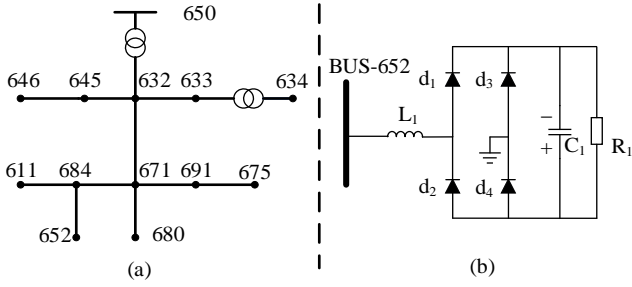


Fig. 7 IEEE-13 Node system with DC load.

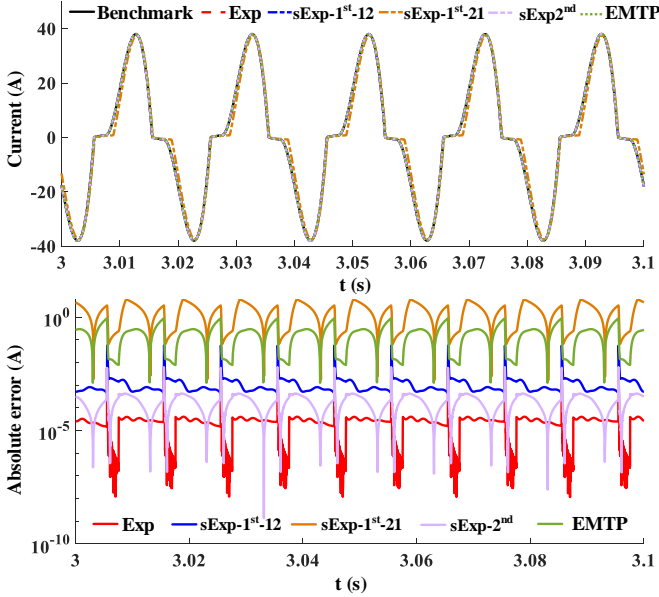


Fig. 8 Comparison of waveforms of the inductor current and the absolute errors.

the sExp-1st-12 scheme. Both are more accurate than EMTP with the same time-step. The sExp-1st-21 scheme has larger absolute errors. It is noted that the sExp-1st-12 and sExp-1st-21 schemes share the same second-order absolute error and the corresponding estimated splitting error is 0.31%, however the third-order absolute errors are 0.34% and 0.28% respectively. In other words, the low-order error is not dominant in this case. The relatively large absolute error of the sExp-1st-12 scheme is due to the miscalculation of switch operations. The estimated splitting error of the sExp-2nd is 0.08%.

B. LLC Resonant Converter

An LLC resonant converter circuit is shown in Fig. 9. The fault resistor is 0.05 m Ω , and the transformer ratio is 1:0.0625. Other parameters are set as in [29]. The IGBTs are modeled as controlled switches with binary resistances. The time-step is 4 ns by evaluating the decoupling error of (17) with a 0.1% threshold. The benchmark waveform is obtained by EMTP with a 1 ns time-step. The simulation lasts for 0.1 s. The dimension of the state equation is 8, which includes the states of the seven inductors and capacitors, respectively, along with the augmented source states, as derived from (2).

Simulation waveforms of the output voltage across the load R_1 , the inductor current of L_2 , the current of the LLC tank and their absolute errors against the benchmark are presented in Fig. 10, where the sExp-1st-12 scheme is abbreviated as sExp-1st. It is shown that the proposed splitting state-space method has good agreements with the benchmark result. The Exp scheme yields the highest accurate results at the same time-step, and it is more accurate than EMTP. The waveforms of absolute errors of the LLC resonant converter reveal that the sExp scheme guarantees enough accuracy under the simulation time-step that meets the splitting error requirement of (17).

The sExp schemes using the first- and second-order accurate approximations are tested under 4 ns and 10 ns time-steps to demonstrate the usage of the inequality (17). The values of splitting errors with sExp-1st and sExp-2nd schemes are listed in Table I. The splitting errors in the table are the maximum ratios considering all switch-dependent variant splitting matrices A_2 . The simulation time-step of 4 ns with a second-order

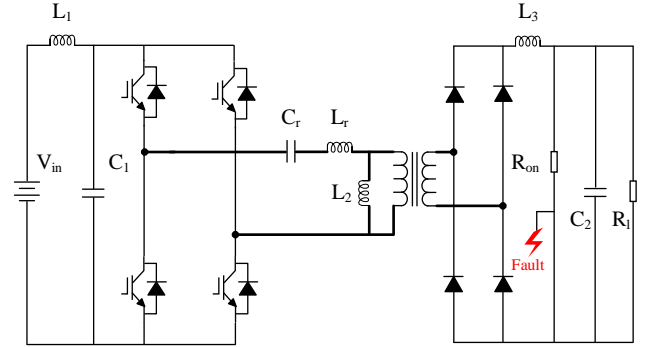


Fig. 9 LLC resonant converter circuit diagram.

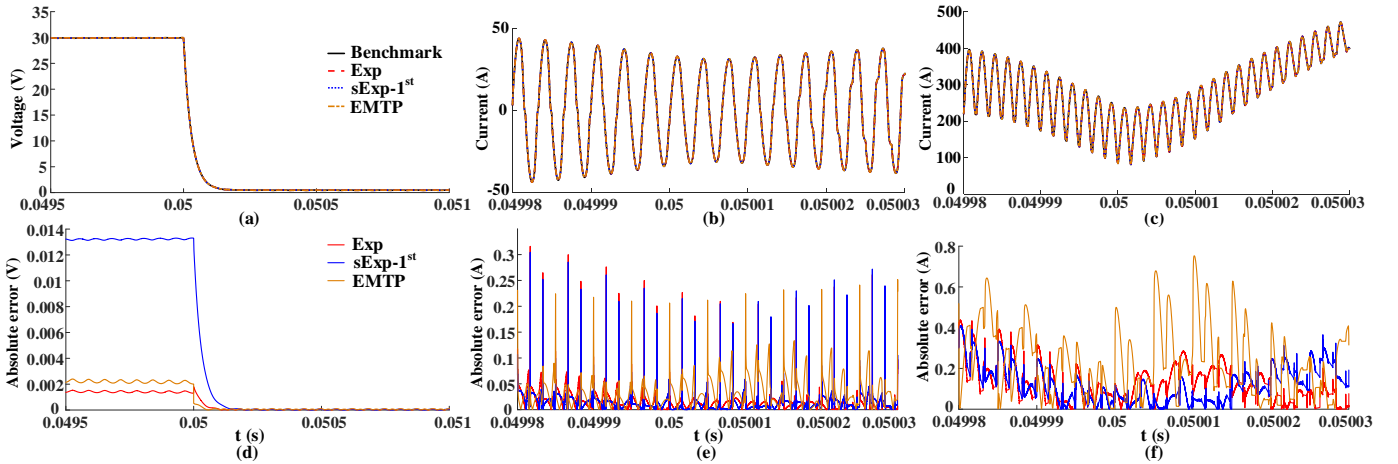


Fig. 10 LLC resonant converter waveforms and absolute errors: (a) R_1 voltage, (b) L_2 current, (c) L_r current, (d)-(f) absolute errors of (a)-(c).

TABLE I

 S_p FOR SPLITTING SCHEMES UNDER DIFFERENT TIME-STEP

Time-step (ns)	Splitting error	
	sExp-1 st	sExp-2 nd
0.5	$8.05e^{-4}$	$9.81e^{-6}$
4	$7.75e^{-3}$	$7.55e^{-4}$
10	$1.94e^{-2}$	$4.74e^{-3}$

accurate splitting scheme satisfies the threshold of 0.1%, while the first-order accurate splitting scheme requires a smaller time-step of 0.5 ns. The LLC resonant converter is usually limited by its volume and the energy storage components are relatively small. Therefore, the measure of the state matrix is dependent on these small time constants. The results demonstrate that a splitting scheme with higher-order accuracy allows a larger time-step size under the same error requirement. In this case, the consumed time associated with numerical integration of the Exp scheme is 56.51 s and the consumed time of sExp-1st scheme is 19.52 s. The speedup of the sExp scheme is 2.89.

C. Wind Farm with Detailed Modeling WTG Unit

A wind farm with type-4 wind turbine generator (WTG) units is tested to further verify the efficiency of the proposed method and compare the accuracy of splitting schemes. As shown in Fig. 11, an extensible number of detailed modeled wind turbine generators are connected to a collector network through linear step-up transformers [30], each of the converters contains 12 IGBT and anti-parallel diode pairs, modeled with binary resistances. The control system of the WTG converter consists of the stator voltage orientation control for the machine side converter and DC voltage and reactive power control for the grid side converter. The collector network includes four feeders modeled by PI-section lines. For the wind farm comprising 50 WTG units, the state equation dimension of the system is 2135, and the dimension of scenarios featuring varying numbers of WTG units scales proportionally to this configuration. The network is subjected to a 3-phase-to-ground fault at $t = 1$ s, which is cleared after 5 cycles. The wind speed is set as 12 m/s, and it changes to 10 m/s at $t = 2$ s. The simulations time-step is $5 \mu\text{s}$, and the benchmark is EMTF results with $1 \mu\text{s}$ time-step.

The simulation results of a 10 WTG units wind farm test are presented first. Fig. 12(a) and (b) show the active power and voltage on the DC side of the back-to-back converter in each

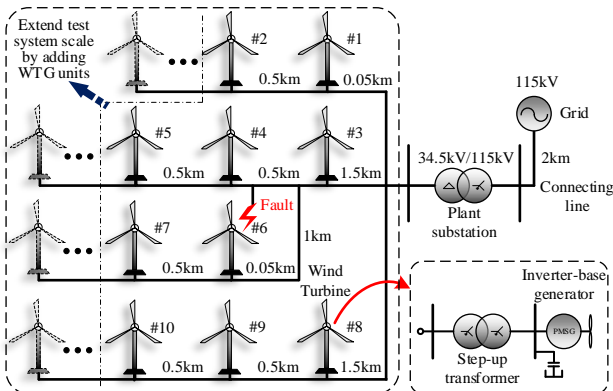


Fig. 11 Diagram of the wind power plant.

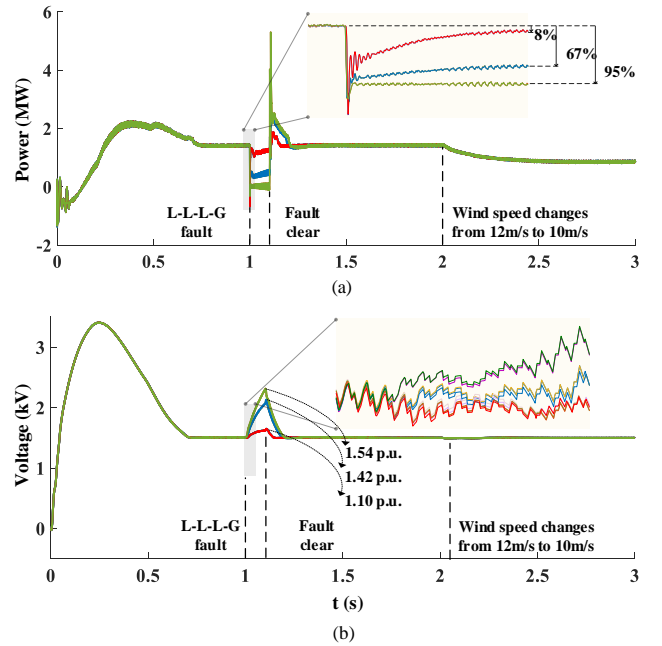


Fig. 12 Waveforms of each WTG unit: (a) active power of each WTG unit, (b) voltage on the DC side of the back-to-back converter.

WTG unit. The ten WTG units of the wind farm are numbered from right to left and from top to bottom, as labeled in Fig. 11. The waveforms of the WTG units can be categorized into three groups, as shown in Fig. 12, based on their relative location to the fault: the active powers of WTG units 1, 2 and 8 to 10 decrease by approximately 8% during the fault and their DC bus voltage increase to 1.10 p.u., the active powers of WTG units 3, 6 and 7 decrease by 67% and their DC bus voltages increase to 1.42 p.u., while the active powers of WTG units 4 and 5 decrease by 95%, and DC bus voltages increase to 1.54 p.u.. Protection system is disabled in this test to observe the natural response of the units.

Next, the numerical errors are compared in detail to assess the accuracy of the presented splitting exponential formulas. The sExp-1st-12, sExp-1st-21, sExp-2nd and Exp schemes are all tested against the benchmark. The absolute error waveform of the output filter currents of the grid-side converter and their zoom-in view are plotted in Fig. 13. The blue and orange lines represent the results of the first-order exponential splitting formulas with different integration orders in the multiple steps integration respectively. It is observed that the error of the sExp-1st-12 scheme is slightly lower than the sExp-1st-21 scheme for the majority of the simulation interval.

The red line represents the results of the second-order accurate scheme sExp-2nd, which shows better accuracy than the blue and orange lines, and almost coincides with the black solid line of the Exp scheme without splitting. The reason is that the Exp scheme possesses second-order accuracy due to the usage of linear interpolation for switching events, while the sExp-2nd scheme has the same order accuracy, and the differences between the third-order error terms are very small.

The execution time of each simulator is shown in Fig. 14. The efficiency of the splitting state-space method is assessed with a series of wind farm tests of an expanding scale, by adding additional WTG units to the feeder line ends separated by

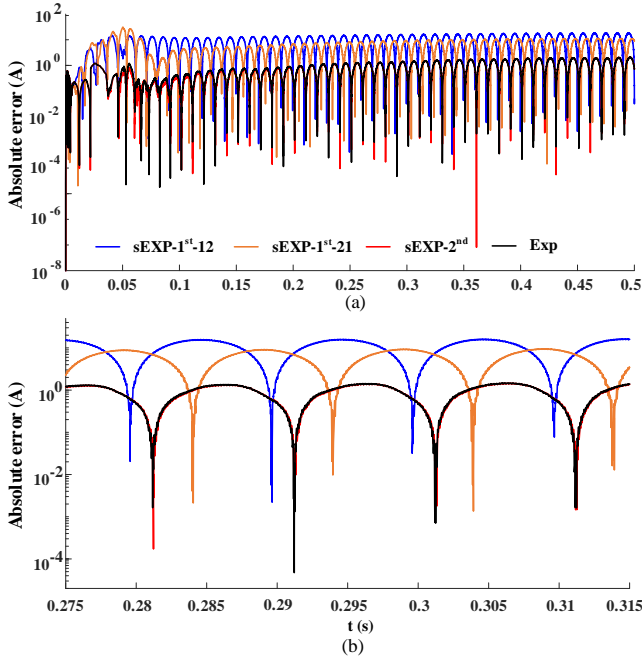


Fig. 13 Error comparisons of first WTG unit: (a) errors of output currents of filter in the back-to-back converter, (b) zoom-in plot of (a).

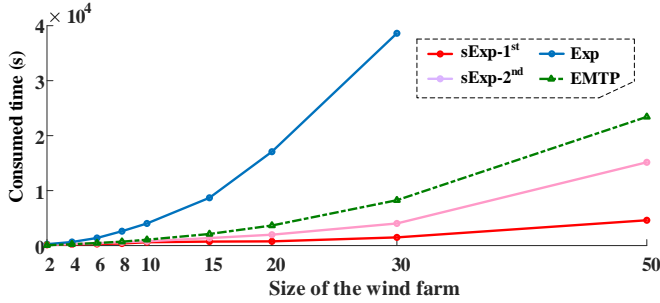


Fig. 14 Consumed time for each scheme.

equidistant PI section lines, as shown in Fig. 11. The CPU times of different scale cases are compared with EMTP on a single core. Switching events interpolations are activated in all exponential integration schemes, and the simultaneous switching option is enabled in EMTP simulations.

Since the integration order does not affect the simulation time, we do not distinguish here the sExp-1st-12 and sExp-1st-21 schemes denoted as sExp-1st in Fig. 14. The consumed time of the tested schemes are listed in TABLE II, and due to the lengthy consumed time for the Exp scheme at 50 WTG units, no further comparisons will be made with it. This scheme drawn in the red solid line achieves more than 2x speedup compared to EMTP drawn in the green dot-dash line, when simulating the wind farm with 20 WTG units. If the scale of the wind farm is expanded to 50 WTG units, the sExp-1st scheme has a more than 3x speedup compared to the EMTP. It is noted that the execution time of the scheme grows quasi-linearly with the simulation scale. The sExp-2nd scheme drawn in the purple solid line gains near 2x speedup against the EMTP for 50 WTG units. The Exp scheme drawn in the blue solid line, which is the original exponential integrator without splitting state-space method and compute all time-varying state matrix exponentials, is less efficient than EMTP, and 26x

TABLE II
PERFORMANCE OF THE WIND FARM CASE

Number of the WTGs	Consumed time (s)			
	EMTP	Exp	sExp-1 st	sExp-2 nd
2	71.09	253.89	134.39	137.77
4	250.90	645.52	209.31	289.18
6	463.83	1382.67	287.25	434.33
8	712.19	1616.20	374.81	605.54
10	1066.14	4027.35	561.11	775.82
20	3654.12	17075.68	768.97	1981.21
30	8255.27	38619.33	1489.33	4026.82
50	24138.12	/	4607.38	15151.93

and 10x slower than the sExp-1st and sExp-2nd schemes respectively. The exponential integration schemes are implemented in MATLAB and have efficiency disadvantages of the scripting language.

D. Modular Multilevel Converter

As another efficiency test of the exponential splitting method, the MMC circuit shown in Fig. 6 with an extensible number of SM each arm, starting from 4 until 200, are studied. The system parameters are given in TABLE III. For 200 SMs in each arm, the number of the state variable of the circuit is 404. The simulation lasts for 0.1 second with a time-step of 20 μ s. The sExp-1st-12 scheme is adopted in the test and referred to as sExp. The sExp scheme is validated with a benchmark result of EMTP with a smaller time-step of 5 μ s.

Detailed comparisons of the 5-level MMC simulation results are given in Fig. 15. The upper and lower arm inductor currents are denoted as i_{upper} and i_{lower} for each scheme. The simultaneous switching function is turned on for the solution in EMTP, with the maximum iteration number set to be 4. From the enlarged views, it can be seen that the accuracy of the sExp scheme is slightly inferior to EMTP and Exp schemes, and they are all consistent with the benchmark.

TABLE III
PARAMETERS OF THE 5-LEVEL MMC CASE

System	Parameters	Values
AC and DC system	AC system RMS voltage	400 kV
	Fundamental frequency	50 Hz
	AC system R/L ratio	10
	DC pole-to-pole voltage	640 kV
	Transformer voltage ratio	400/320
	Transformer rated power	1000 MVA
	Transformer reactance	0.18 p.u.
MMC	Transformer resistance	0.001 p.u.
	Capacitor energy in each SM	40 kJ/MVA
	Number of SMs per arm	4 - 200
	MMC arm inductance	0.15 p.u.

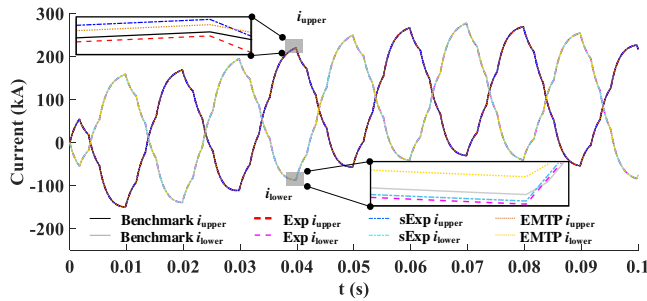


Fig. 15 Waveforms of the currents of the upper and lower arm inductors.

TABLE IV
PERFORMANCE OF THE MMC CASE FOR 0.1 SECOND SIMULATION

Voltage Levels	5	11	21	51	101	201
Speedup	1.06	1.30	1.37	2.55	6.18	16.63

The speedups of the sExp scheme are listed in TABLE IV. The speedups are computed by comparing with the Exp scheme. For the 5-level MMC case, the sExp and Exp schemes have similar execution time. As the number of voltage levels in the MMC circuit increases, the speedups of the sExp scheme over the Exp scheme gradually increases. At 201 levels, the speedup ratio reaches 16.63.

V. CONCLUSION

This paper has presented a splitting state-space method with a decoupling principle for converter-integrated power systems electromagnetic transient simulations. The splitting state-space method is established with different order exponential splitting formulas applied to the time-variant state-space matrices of power converter EMT models, which separate each integration step into multiple stages, and avoid recurring computation of the matrix exponential functions. Furthermore, a criterion to estimate the induced splitting error is given to suggest appropriate time-step size for splitting method simulations. A generic decoupling principle is then introduced and demonstrated on common converter topologies. By collecting the time-variant parts of the state matrix and coordinating the various order accuracy approximations of the splitting state-space method, the computational burden brought by high frequency switching transients of converter-integrated power systems is effectively suppressed, by avoiding repeated matrix exponential calculations.

An IEEE-13 node system with DC load, an LLC resonant converter case, a large-scale wind farm case and an MMC case have verified that the proposed method provides adjustable order accurate results, and gains speedups against the traditional methods, especially for power system integrated with many power converters, such as studies involving the detailed modeled wind farms. Works in exploiting the parallelism in the proposed splitting state-space method for converter-integrated system simulations and acceleration via GPU computing to further improve efficiency is under development.

REFERENCES

[1] W. Du et al., "Modeling of grid-forming and grid-following inverters for dynamic simulation of large-scale distribution systems," *IEEE Trans. Power Del.*, vol. 36, no. 4, pp. 2035–2045, Aug. 2021.

[2] U. Karaagac, J. Mahseredjian, L. Cai, and H. Saad, "Offshore wind farm modeling accuracy and efficiency in MMC-based multiterminal HVDC connection," *IEEE Trans. Power Del.*, vol. 32, no. 2, pp. 617–627, Apr. 2017.

[3] H. Li, J. Shair, J. Zhang and X. Xie, "Investigation of subsynchronous oscillation in a DFIG-based wind power plant connected to MTDC grid," *IEEE Trans. Power Syst.*, vol. 38, no. 4, pp. 3222–3231, Jul. 2023.

[4] Y. Shu, G. Tang, and H. Pang, "A back-to-back VSC-HVDC system of Yu-E power transmission lines to improve cross-region capacity," *CSEE J. Power Energy Syst.*, vol. 6, no. 1, pp. 64–71, Mar. 2020.

[5] H. Chalanger, T. Ould-Bachir, K. Sheshyekani, and J. Mahseredjian, "Methods for the accurate real-time simulation of high-frequency power converters," *IEEE Trans. Ind. Electron.*, vol. 69, no. 9, pp. 9613–9623, Sept. 2022.

[6] M. Ouafi, Jean Mahseredjian, J. Peralta, H. Gras, S. Denetiere, and B. Bruned, "Parallelization of EMT simulations for integration of inverter-based resources", *Electric Power Syst. Res.*, Vol. 223, Oct. 2023.

[7] F. A. Moreira, J. R. Marti, L. C. Zaneta, and L. Linares, "Multirate simulations with simultaneous-solution using direct integration methods in a partitioned network environment," *IEEE Trans. Circuits Syst. I, Reg. Papers*, vol. 53, no. 12, pp. 2765–2778, Dec. 2006.

[8] B. Bruned, J. Mahseredjian, S. Denetiere, J. Michel, M. Schudel, and N. Bracikowski, "Compensation method for parallel and iterative real-time simulation of electromagnetic transients," *IEEE Trans. Power Deliv.*, vol. 38, no. 4, pp. 2302–2310, Aug. 2023.

[9] C. Dufour, "Highly stable rotating machine models using the state-space-nodal real-time solver," in *Proc. IEEE Workshop Complexity Eng.*, 2018.

[10] T. Kato, K. Inoue, T. Ogawa, and Y. Takami, "Automatic circuit partitioning for parallel processing of power electric system simulation," *IEEE Trans. Ind. Appl.*, vol. 135, no.10, pp. 1025, 2015.

[11] C. Jin, Z. Ji, K. Liu, W. Chen, and J. Zhao, "A region-folding electromagnetic transient simulation approach for large-scale power electronics system," *IEEE Trans. Power Electron.*, vol. 38, no. 8, pp. 9755–9766, Aug. 2023.

[12] P. Pejovic and D. Maksimovic, "A new algorithm for simulation of power electronic systems using piecewise-linear device models," *IEEE Trans. Power Electron.*, vol. 10, no. 3, pp. 340–348, May 1995.

[13] S. Y. R. Hui and C. Christopoulos, "A discrete approach to the modeling of power electronic switching networks," *IEEE Trans. Power Electron.*, vol. 5, no. 4, pp. 398–403, Oct. 1990.

[14] Q. Mu, J. Liang, X. Zhou, Y. Li, and X. Zhang, "Improved ADC model of voltage-source converters in dc grids," *IEEE Trans. Power Electron.*, vol. 29, no. 11, pp. 5738–5748, Nov. 2014.

[15] K. Wang, J. Xu, G. Li, N. Tai, A. Tong, and J. Hou, "A generalized associated discrete circuit model of power converters in real-time simulation," *IEEE Trans. Power Electron.*, vol. 34, no. 3, pp. 2220–2233, Mar. 2019.

[16] S. Yu, S. Zhang, Y. Han, Y. Wei, and S. Zou, "A pulse-source-pair-based AC/DC interactive simulation approach for multiple-VSC grids," *IEEE Trans Power Deliv.*, vol. 36, no. 2, pp. 508–521, Apr. 2021.

[17] H. Saad, J. Peralta, S. Denetiere, and J. Mahseredjian, "Dynamic averaged and simplified models for MMC-based HVDC transmission systems", *IEEE Trans. Power Deliv.*, vol. 28, no. 3, pp. 1723–1730, Jun. 2013.

[18] C. Wang, X. Fu, P. Li, J. Wu, and L. Wang, "Multiscale simulation of power system transients based on the matrix exponential function," *IEEE Trans. Power Syst.*, vol. 32, no. 3, pp. 1913–1926, May 2017.

[19] M. Hochbruck and A. Ostermann, "Exponential integrators," *Acta Numer.*, vol. 19, pp. 209–286, May 2010.

[20] E. Hairer, C. Lubich, and G. Wanner, *Geometric Numerical Integration*, 2nd ed., Springer, 2001.

[21] H. F. Trotter, "On the product of semi-groups of operators," *Proc. Am. Math. Soc.*, vol. 10, pp. 545–551, 1959.

[22] R. I. McLachlan and G. Quispel, "Splitting methods," *Acta Numer.*, vol. 11, pp. 341–434, 2002.

[23] N. Hatano and M. Suzuki, "Finding exponential product formulas of higher orders," in *Quantum Annealing and Other Optimization Methods*, A. Das and B. K. Chakrabarti, Eds. Berlin, Germany: Springer, 2005.

[24] L. F. Shampine and H. A. Watts, "Global error estimates for ordinary differential equations," *ACM Trans. Math. Softw.*, vol. 2, no. 2, pp. 172–186, 1976.

[25] T. Ström, "On logarithmic norms," *SIAM J. Numer. Anal.*, vol. 12, pp. 741–753, 1975.

- [26] R. J. LeVeque and J. Olinger, "Numerical methods based on additive splittings for hyperbolic partial differential equations," *Math. Comput.*, vol. 40, no. 162, pp. 169-497, 1983.
- [27] J. Xu, Y. Zhao, C. Zhao and H. Ding, "Unified high-speed EMT equivalent and implementation method of MMCs with single-port submodules," *IEEE Trans. Power Deliv.*, vol. 34, no. 1, pp. 42-52, Feb. 2019.
- [28] J. Mahseredjian, S. Denetière, L. Dubé, B. Khodabakhchian, and L. Gérin-Lajoie, "On a new approach for the simulation of transients in power systems". *Electr. Power Syst. Res.*, vol. 77, no. 11, pp. 1514-1520, Sept. 2007.
- [29] W. Nzale, J. Mahseredjian, X. Fu, I. Kocar, and C. Dufour, "Improving numerical accuracy in time-domain simulation for power electronics circuits," *IEEE Open Access J. Power Energ.*, vol. 8, pp. 157-165, 2021.
- [30] D.N. Hussein, M. Mahmoud, and R. Iravani, "A type-4 wind power plant equivalent model for the analysis of electromagnetic transients in power systems," *IEEE Trans. Power Syst.*, vol. 28, pp. 3096-3104, Aug. 2013.



Xiaopeng Fu (Member, IEEE) received the B.S. and Ph.D. degree in electrical engineering from Tianjin University, Tianjin, China, in 2011 and 2016, respectively.

He was a Postdoctoral Fellow in Power Systems Department, Polytechnique de Montreal, Montreal, Canada, in 2007. He is currently an Associate Professor with the School of Electrical and Information Engineering, Tianjin University. His current research interests include analysis of distributed generation system, microgrid, and simulation of electromagnetic transients. He is a member of the Chinese Society for Electrical Engineering.



Wei Wu (Member, IEEE) received the B.S., M.Sc., and Ph.D. degrees in electrical engineering from Tianjin University, Tianjin, China, in 2017, 2020, and 2024, respectively.

He is currently an assistant researcher with the Beijing Huairou Laboratory. His research interests include analysis of distributed generation system, microgrid, electromagnetic transient simulation, and parallel computing.



Peng Li (Senior Member, IEEE) received the B.S. and Ph.D. degrees in electrical engineering from Tianjin University, Tianjin, China, in 2004 and 2010, respectively.

He is currently a Professor with the School of Electrical and Information Engineering, Tianjin University. His current research interests include operation and planning of active distribution networks, modeling, and transient simulation of power systems. He is an Associate Editor of *IEEE TRANSACTIONS ON SUSTAINABLE ENERGY*, *CSEE Journal of Power and Energy Systems*, *Sustainable Energy Technologies and Assessments*, and *IET Renewable Power Generation*.



Jean Mahseredjian (Fellow, IEEE) received the Ph.D. degree in electrical engineering from Polytechnique Montréal, Montreal, QC, Canada, in 1991.

From 1987 to 2004, he was with IREQ (Hydro-Québec) working on research and development activities related to the simulation and analysis of electromagnetic transients. In December 2004, he joined the Faculty of Electrical Engineering, Polytechnique Montréal.



Jianzhong Wu (Fellow, IEEE) received the B.Sc., M.Sc., and Ph.D. degrees in electrical engineering from Tianjin University, China, in 1999, 2002, and 2004, respectively. From 2004 to 2006, he was with Tianjin University, where he was an Associate Professor. From 2006 to 2008, he was a Research Fellow with the University of Manchester, Manchester, U.K. He is a Professor of Multi-Vector Energy Systems and the Head of the School of Engineering, Cardiff University, U.K. His research interests include integrated multi-energy infrastructure and smart grid. He is Co-Editor-in-Chief of *Applied Energy* and the Co-Director of U.K. Energy Research Centre and EPSRC Supergen Energy Networks Hub.

He is Co-Editor-in-Chief of *Applied Energy* and the Co-Director of U.K. Energy Research Centre and EPSRC Supergen Energy Networks Hub.



Chengshan Wang (Senior Member, IEEE) received the Ph.D. degree in electrical engineering from Tianjin University, Tianjin, China, in 1991.

He is currently a Professor with the School of Electrical and Information Engineering, Tianjin University, where he is the Director of the Key Laboratory of Smart Grid, Ministry of Education. His research interests include distribution system analysis and planning, distributed generation system, and microgrid. He is the Editor-in-Chief of *IET Energy Systems Integration* and a Member of the Chinese Academy of Engineering.